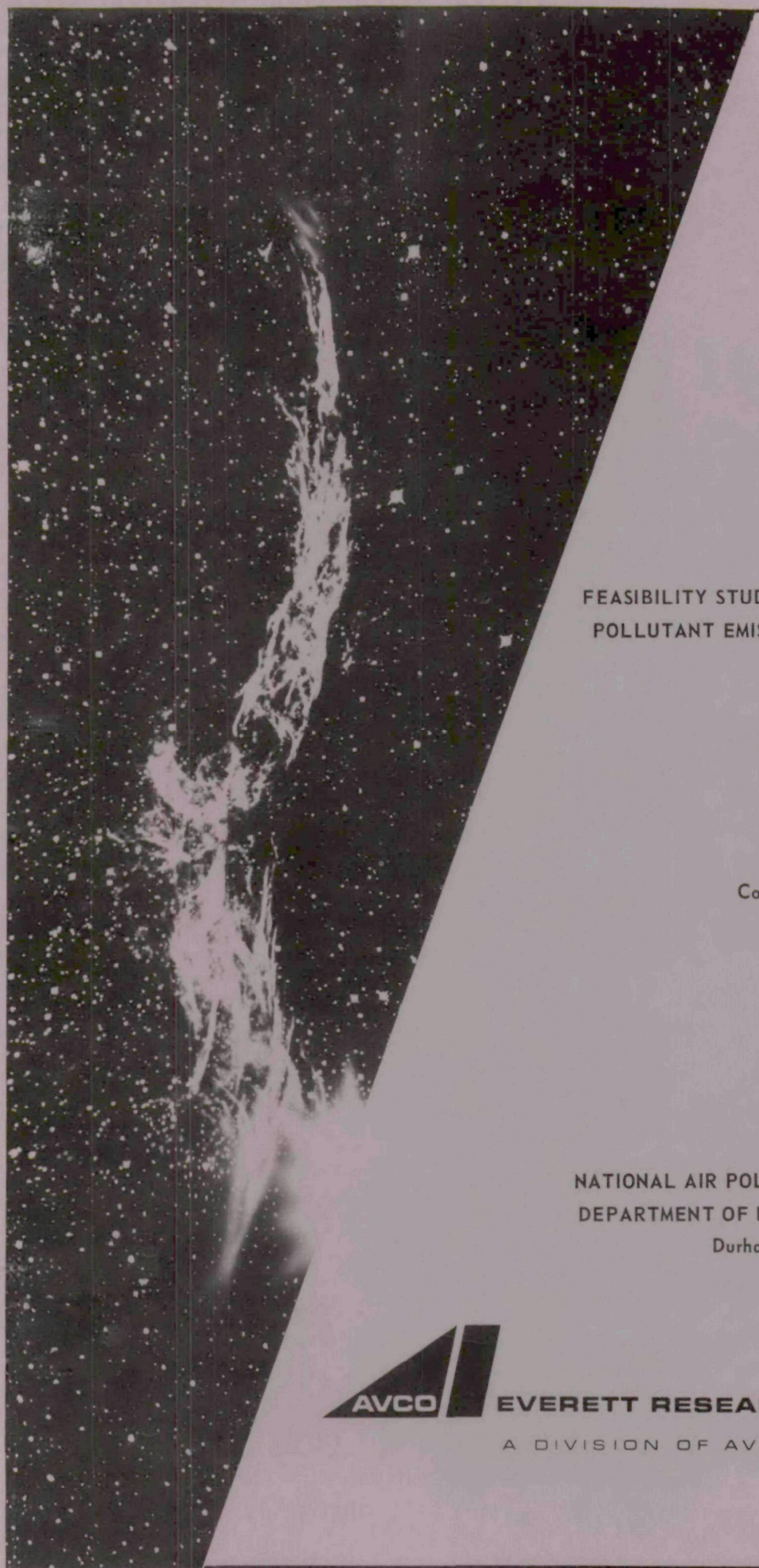

# FEASIBILITY STUDY OF REMOTE MONITORING OF GAS POLLUTANT EMISSIONS BY RAMAN SPECTROSCOPY

## FINAL REPORT

Donald A. Leonard

Contract CPA 22-69-62
November 1970

prepared for

NATIONAL AIR POLLUTION CONTROL ADMINISTRATION
DEPARTMENT OF HEALTH, EDUCATION AND WELFARE
Durham, North Carolina 27701

AVCO EVERETT RESEARCH LABORATORY
A DIVISION OF AVCO CORPORATION

# FEASIBILITY STUDY OF REMOTE MONITORING OF GAS POLLUTANT EMISSIONS BY RAMAN SPECTROSCOPY

FINAL REPORT

by

Donald A. Leonard

AVCO EVERETT RESEARCH LABORATORY
a division of
AVCO CORPORATION
Everett, Massachusetts

Contract CPA 22-69-62

November 1970

prepared for

NATIONAL AIR POLLUTION CONTROL ADMINISTRATION
DEPARTMENT OF HEALTH, EDUCATION AND WELFARE
Durham, North Carolina 27701

TABLE OF CONTENTS


| | | Page |
|---|---|---|
| | *List of Illustrations* | v |
| I. | INTRODUCTION | 1 |
| II. | RAMAN SCATTERING THEORY | 3 |
| III. | MEASUREMENT OF NO AND $SO_2$ RAMAN SCATTERING CROSS-SECTIONS | 11 |
| IV. | NUMERICAL BASIS FOR POWER PLANT PLUME FIELD EXPERIMENTS | 13 |
| V. | EXPERIMENTAL FIELD APPARATUS | 21 |
| VI. | EXPERIMENTAL FIELD RESULTS | 31 |
| VII. | CONCLUSIONS | 39 |
| VIII. | RECOMMENDATIONS | 41 |
| | REFERENCES | 42 |
| | APPENDIX - MEASUREMENT OF NO AND $SO_2$ RAMAN SCATTERING CROSS-SECTIONS | A-1 |
| | APPENDIX REFERENCES | A-6 |

## LIST OF ILLUSTRATIONS


| Figure | | Page |
|---|---|---|
| II-1 | Potential energy diagram for diatomic molecule undergoing vibrational Raman scattering. | 4 |
| II-2 | Detailed structure of the vibrational Raman line for $N_2$ at T = 300°K showing the close overlap of the $\Delta J = 0$ transitions and the production of sidebands by the $\Delta J = \pm 2$ transitions. | 7 |
| II-3 | Apparent change in signal as a function of temperature with various fixed wavelength aperatures in the detection system. | 9 |
| IV-1 | Concentration of pollutant detectable as a function of range and integration time. | 15 |
| IV-2 | Typical Raman spectrum from combustion gases using a 3371 Å laser source. | 18 |
| V-1 | Optical system used in the power plant field experiment | 22 |
| V-2 | Transmission characteristic of the liquid filter used in the optical system of the field experiment. | 24 |
| V-3 | Schematic of the photon counting electronic detection system. | 25 |
| V-4 | Schematic of the 10-channel photon counting detection system. | 27 |
| V-5 | Plan view of the Boston Edison Mystic Station showing the position of the laser Raman spectrometer van. | 28 |
| V-6 | Photograph of spectrometer van at power plant site. | 29 |
| VI-1 | Remote ambient air Raman spectrum. | 32 |
| VI-2 | Raman spectrum of smoke plume showing spontaneous emission lines. | 33 |
| VI-3 | Raman spectrum of smoke plume with spontaneous emission lines suppressed. | 34 |

| Figure | | Page |
|---|---|---|
| VI-4 | Plume profile showing normalized Raman scattering from $N_2$, $O_2$, $CO_2$ and $H_2O$. | 36 |
| VI-5 | Water vapor to oxygen Raman ratio in ambient air. | 38 |
| A-1 | Schematic of experimental arrangement for $90^o$ cross-section measurements. | A-2 |
| A-2 | Schematic of experimental arrangement for $180^o$ cross-section measurements. | A-4 |
| A-3 | Spectral scan of 50% NO - 50% $N_2$ mixture showing the relative strength of the NO line at 3599 Å and the $N_2$ line at 3658 Å. | A-5 |

# I. INTRODUCTION

This report describes work performed between 2 June 1969 and 1 August 1970 under Contract CPA22-69-62, "Feasibility Study of Remote Monitoring of Gas Pollutant Emissions by Raman Spectroscopy," supported by the National Air Pollution Control Administration.

The specific objective of this contract has been to determine the feasibility of using laser Raman scattering to remotely monitor the emission of NO and $SO_2$ from large stationary sources such as electric power plants. The work has been divided into two phases as discussed below.

PHASE I - Controlled Laboratory Study: The first phase concentrated primarily on the measurement of the Raman scattering cross-sections for NO and $SO_2$, since no previous measurement of these cross-sections was known to have been made. Knowledge of these cross-sections is essential both to evaluate the feasibility of the method and to quantitatively calibrate the instrumentation. The cross-sections for both NO and $SO_2$ were satisfactorily measured in the Laboratory and the results have been published in the Journal of Applied Physics.

PHASE II - Field Evaluation: The second phase has been devoted to an evaluation of the feasibility of the method in the field on an actual source of pollutant emissions. The Boston Edison, Mystic Station Electric Power Plant, located a mile from the Avco Everett Research Laboratory, was selected for the field study. A laser Raman spectrometer utilizing a 3371 Å pulsed nitrogen laser was installed in a van at the plant site, and considerable data have been collected.

For the first time, Raman spectra of $N_2$, $O_2$, $H_2O$ and $CO_2$ have been obtained from a power plant plume without interference, and detailed field procedures have been developed which permit quantitative

profiles of the molecular density of these molecules in the plume to be routinely obtained. However, NO and $SO_2$ have not yet been observed, due primarily to the insufficient stray light rejection ratio of the monochrometer used in the present system.

The important conclusion to date is that no evidence has yet been obtained which shows that the method will not work. However, a conclusive proof of the feasibility of the method has yet to be established. Improvement in the monochrometer quality will allow the feasibility of the method to be conclusively resolved.

Other improvements in S/N include the possibility of focusing the laser to increase beam brightness at the plume and the substitution of non-dispersive wavelength selection to reduce the loss of Raman signal by the monochrometer slit field stop.

## II. RAMAN SCATTERING THEORY

### A. History

In 1923, Smekal[1] published a theoretical paper on the quantum theory of dispersion in which he showed that for light scattering in transparent media frequencies other than those present in the original light might be found in the scattered radiation. The effect predicted by Smekal was experimentally verified in liquids by Raman in 1928, and the phenomenon is now known as the Raman effect.

For several decades Raman spectroscopy proved to be an invaluable tool of the physicist for studying the structure of molecules. However, this early work was limited by the need for very long exposure times with extremely high power mercury arc lamps. The advent of the laser, a high intensity source of monochromatic light, has caused a renewed interest in Raman spectroscopy. Instruments have been marketed which combine CW lasers and scanning tandem monochromators into systems of great practical utility for laboratory use. The intent of this effort was to study the feasibility of extending the practical application of Raman scattering for the remote analysis of power plant plumes in field situations.

### B. Theory

The frequencies observed in Raman scattering correspond to the frequency of the incident light shifted by some characteristic frequency of the scattering molecule. A potential energy diagram for a typical molecule undergoing vibrational Raman scattering is shown in Fig. II-1. Photons of frequency $\nu_o$ and energy $h\nu_o$ are incident on the molecule. Photons of frequency $\nu_{Raman}$ and energy $h\nu_{Raman}$ are scattered, and the molecule is left in a higher vibrational energy state after the collision than before. The difference in energy between the incident and scattered photons is exactly equal to the energy given to the molecule,

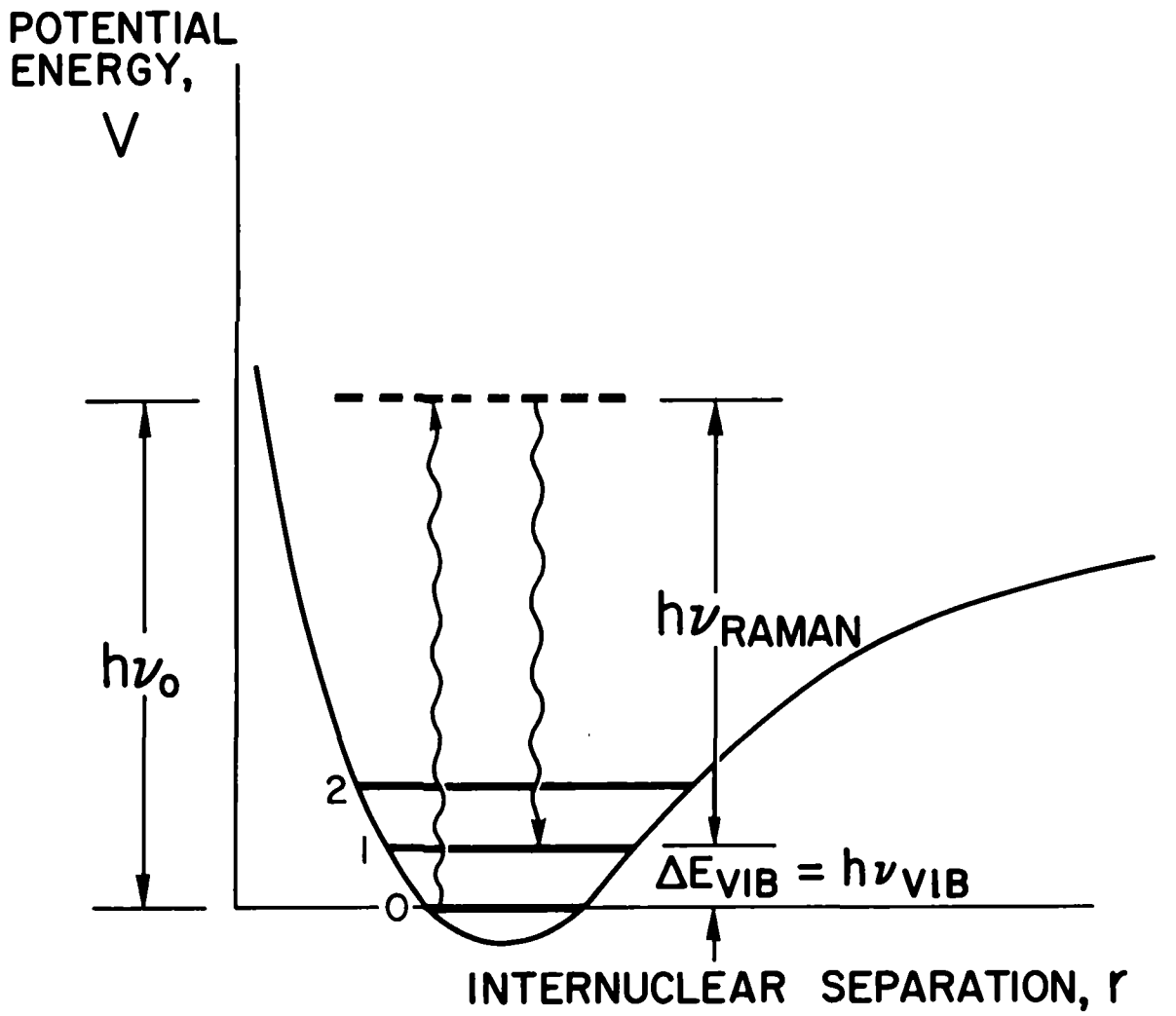


$$h\nu_{RAMAN} = h\nu_o - \Delta E_{VIB}$$

Fig. II-1 Potential energy diagram for diatomic molecule undergoing vibrational Raman scattering.

and in the case of vibrational excitation, is the vibrational energy spacing, $\Delta E_{Vib}$. Thus, by measuring the energy of the Raman scattered photons and by knowing the energy of the incident photons the vibrational energy spacing of the scattering molecule may be determined. Conversely, if the energy of Raman photons from a particular molecular species is known, then a measurement of the Raman scattering at that photon energy will be a means of monitoring that particular species.

The molecular species of importance for atmospheric Raman scattering are listed in Table I. The vibrational energy spacing, the wavelength to which the Raman scattering is shifted (assuming a 3371 Å pulsed nitrogen laser source) and the Raman scattering cross-section for each species, normalized to nitrogen, are also shown.

The selection rules for the change in rotational-quantum number during a vibration Raman transition are $\Delta J = 0$ and $\Delta J = \pm 2$. Usually all the lines having $\Delta J = 0$ lie very close to each other in energy and are not resolved except with very high resolution spectroscopy. The $\Delta J = \pm 2$ transitions, however, are well separated in energy and appear as side bands on either side of the intense $\Delta J = 0$ line. Figure II-2 is a representation of the vibrational Raman scattering for molecular nitrogen excited with a 3371 Å pulsed nitrogen laser, showing the intense $\Delta J = 0$ line with much weaker side bands for the $\Delta J = -2$ and $\Delta J = +2$ rotational transitions.

This figure was drawn for a temperature of 300°K with the assumption that the $\Delta J = 0$ transition is a factor of 100 stronger than the $\Delta J = \pm 2$ transitions, as indicated by a theoretical calculation by Sharma.[2] Details such as the alternation in intensity of the $\Delta J = +2$ lines have been neglected. See Herzberg[3] for further information.

The side bands can be important in practice for the following two reasons:

(1) The $\Delta J = \pm 2$ side bands of a strongly scattering, high concentration species may overlap and mask the weaker $\Delta J = 0$ scattering from a low concentration species. This does not appear to be a problem for the detection of NO and $SO_2$ which are well separated in Raman energy shift from $N_2$ and other high concentration species. However, problems

TABLE I

DATA FOR MOLECULAR SPECIES OF INTEREST
FOR ATMOSPHERIC RAMAN SCATTERING

| Molecule | Vibrational Energy Spacing | Wavelength of Raman Scattering with 3371 Å Laser Source | $\frac{\sigma_{RAMAN}}{\sigma_{RAMAN\ (N_2)}}$ |
|---|---|---|---|
| $N_2$ | 2330 $cm^{-1}$ | 3658 Å | 1.00 |
| $O_2$ | 1556 | 3558 | 1.5* |
| $H_2O$ | 3652 | 3844 | 4.15** |
| $CO_2$ | 1285.5 | 3523.7 | 2.2*** |
| | 1388.3 | 3536.5 | 2.2 |
| CO | 2143 | 3634 | - |
| NO | 1876 | 3599 | 0.5**** |
| $SO_2$ | 1151 | 3507 | 2.4**** |

* Widhopf and Lederman (Brooklyn Polytech) see Reference 4

** Cooney, NCAR - Reference 5

*** Derr, ESSA - Reference 6

**** Leonard, Avco - Reference 7 and Section III

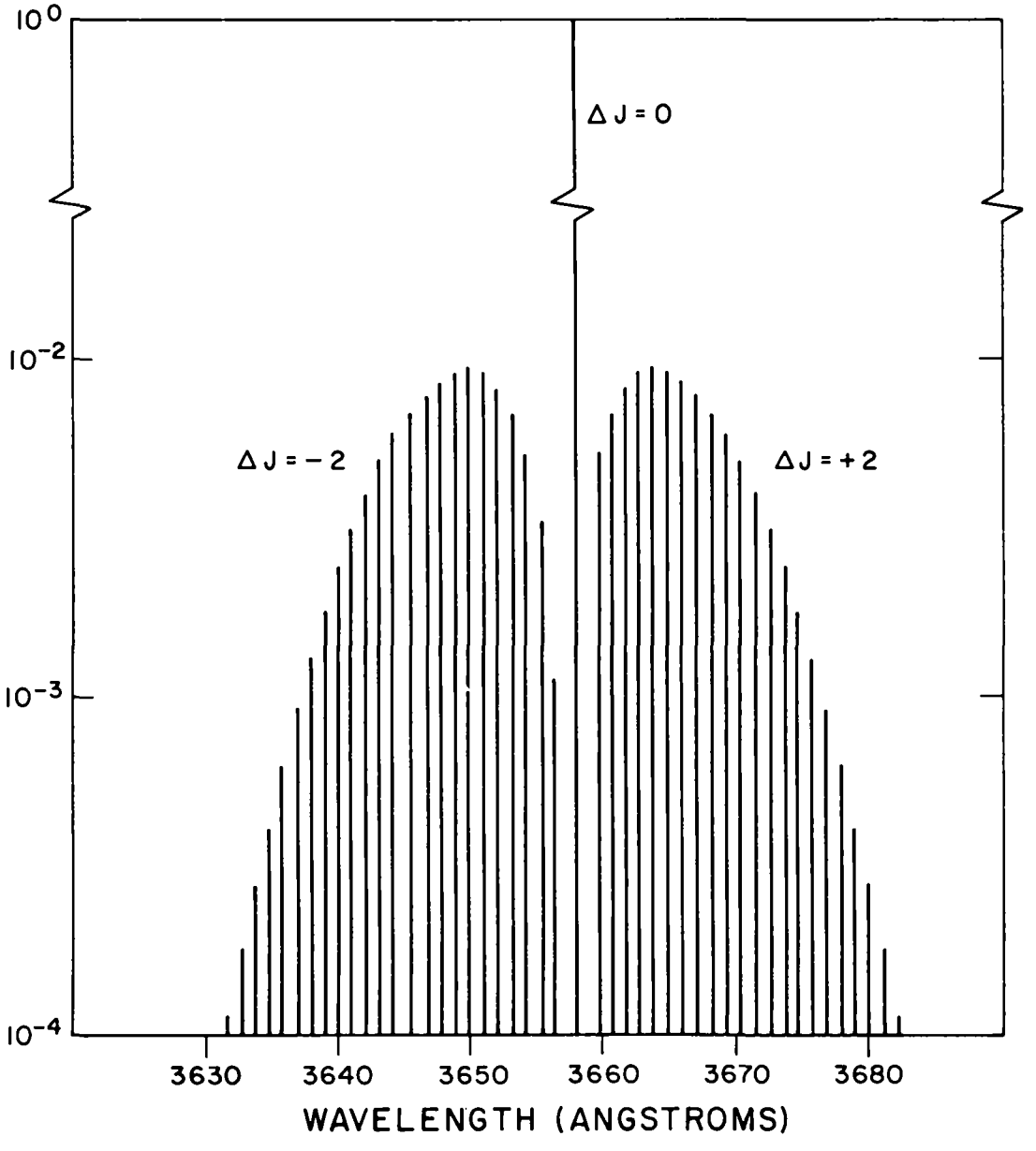


Fig. II-2 Detailed structure of the vibrational Raman line for $N_2$ at $T = 300^{\circ}K$ showing the close overlap of the $\Delta J = 0$ transitions and the production of sidebands by the $\Delta J = \pm 2$ transitions.

may arise in cases such as the detection of trace amounts of CO in the presence of high concentrations of $N_2$, as in combustion plumes. This potential source of interference in the analysis of combustion plumes due to side bands is discussed in more detail in Section IV.

(2) With a fixed wavelength aperture in the detection system, temperature variations will cause changes in the amount of Raman scattering detected from a constant density of scattering molecules. This is illustrated by Fig. II-3 which shows the fraction of the total Raman scattering from $\Delta J = 0$ and $\Delta J = \pm 2$ as a function of temperature for various fixed wavelength aperture widths which are centered on the $\Delta J = 0$ line. This plot is calculated theoretically for the worst case when the strength of the $\Delta J = \pm 2$ transitions are assumed equal to the $\Delta J = 0$. It can be noted that for very wide apertures which include most of the side bands there is very little temperature effect and also for very narrow apertures there is also very little temperature effect. Precision measurements at the 1% level of accuracy may have to take this effect into consideration.

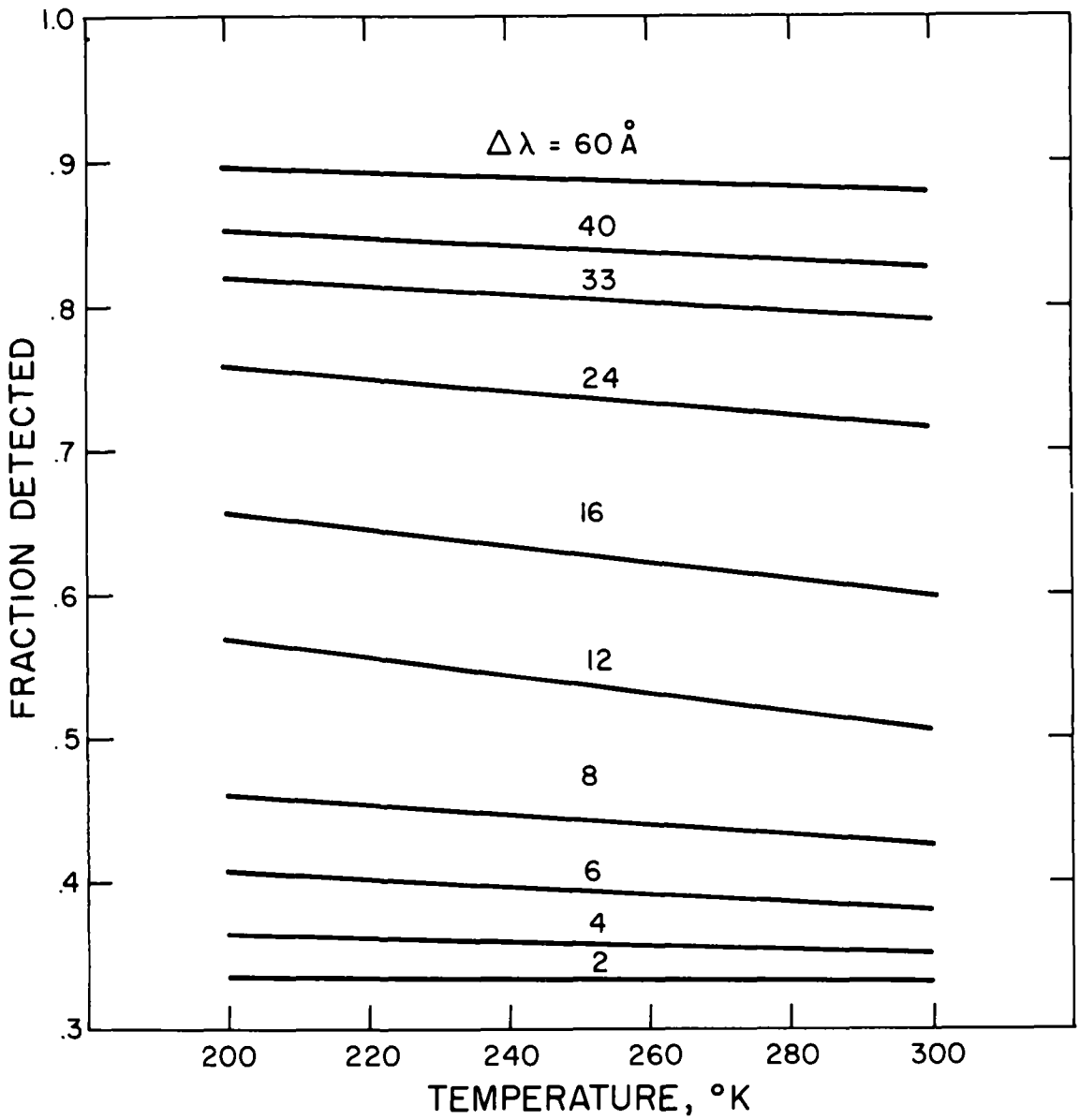


Fig. II-3 Apparent change in signal as a function of temperature with various fixed wavelength aperatures in the detection system.

## III. MEASUREMENT OF NO AND $SO_2$ RAMAN SCATTERING CROSS-SECTIONS

The Raman scattering cross-sections for NO and $SO_2$ were measured experimentally with a 3371 Å laser source as part of this feasibility study, since no previous measurements of these cross-sections was known to have been made.

The results of these measurements has been published in the Journal of Applied Physics. The text of this paper is reproduced as an Appendix to this report.

Additional information which was not included in the paper as published:

1. The measurements were carried out at room temperature, i. e., approximately 300°K.
2. The instrumental bandpass was 17 Å as controlled by a 1 mm slit on a 1/2-meter 1200 ℓ/mm grating monochrometer.
3. The results were corrected for spectrometer, interference filter and photomultiplier spectral response which over the 151 Å range between the $SO_2$ line at 3507 Å and the $N_2$ line at 3658 Å amounted to 30% or less.
4. The quoted uncertainties were the combination of the photostatistic and spectral response uncertainties.

## IV. NUMERICAL BASIS FOR POWER PLANT PLUME FIELD EXPERIMENTS

The number of Raman photoelectrons collected by an optical detector in an atmospheric pulsed laser backscattering system can be expressed by the following range equation:

$$N_{PE} = N_{LASER} f t N_{SCAT} \sigma_{RAMAN} \Delta R \frac{A_T}{R^2} \epsilon_{pe} \epsilon_{op} T_{\lambda} T_{\lambda_2}$$

where $N_{PE}$ = number of Raman photoelectrons detected

$N_{LASER}$ = number of laser photons per pulse

$f$ = laser pulse repetition frequency

$t$ = integration time

$N_{SCAT}$ = density of molecular scatters

$\sigma_{RAMAN}$ = Raman scattering cross-section per particle per steradian

$\Delta R$ = range resolution

$A_T$ = telescope aperture area = $\frac{\pi D^2}{4}$

$D$ = telescope aperture diameter

R= range

$\epsilon_{pe}$ = photocathode photoelectric efficiency

$\epsilon_{op}$ = optical system efficiency

$T_{\lambda_1} T_{\lambda_2}$ = two-way atmospheric transmission, $T_{\lambda_1}$ at laser wavelength and $T_{\lambda_2}$ at Raman wavelength

It can be seen from this equation that, if the transmitter and receiver system parameters $N_{LASER}$, $\sigma_{RAMAN}$, $\Delta R$, the detection solid angle and the detection efficiencies are known, the only two quantities remaining are the density of scattering molecules $N_{SCAT}$ and the two-way transmission factor $T_{\lambda_1} T_{\lambda_2}$ to the range of interest. Thus a measure of the Raman scattering from a single range cell can be used to determine directly the product of the density of scatterers and the two-way transmission to the region of interest.

If the density of one component, such as $N_2$ is known, a measure of its Raman scattering yields the transmission to the range cell of interest. Thus, normalization of the Raman scattering from pollutants of unknown concentration to that of $N_2$ yields an absolute concentration ratio independent of transmission, if the transmission at the various Raman wavelengths differs only slightly.

A calculation was carried out using the above range equation with system parameters which assume state-of-the-art, well engineered components. The parameters assumed are listed below together with a brief rationale for the particular choice.

The detectable concentration of NO and $SO_2$ as calculated using the above range equation and system parameters is shown in Fig. IV-1 as a function of range and integration time. The conclusion from this figure is that NO and $SO_2$ should be detectable at the 100 PPM level at ranges up to 1000 feet with reasonable integration times the order of a few minutes.

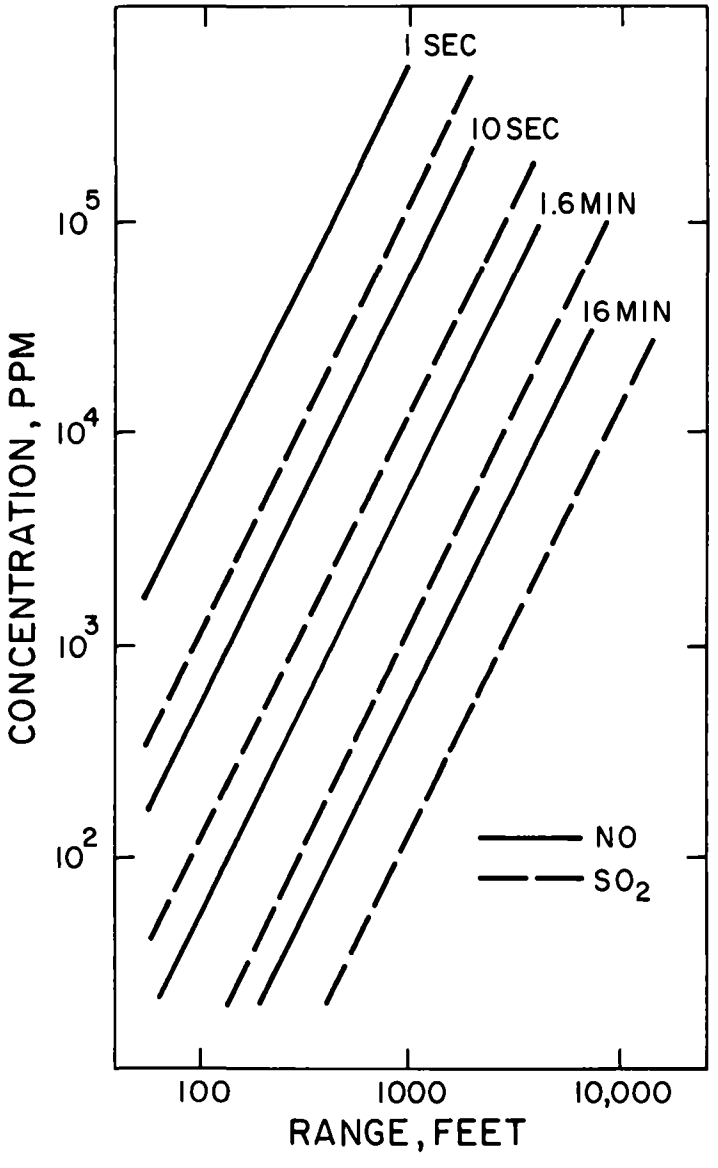


Fig. IV-1 Concentration of pollutant detectable as a function of range and integration time.

| System Parameter | Value Assumed | Rational |
|---|---|---|
| $N_{PE}$ | 100 photoelectrons | In a signal limited situation, such as during night operation, this would produce a photostatistical accuracy of 10%. |
| $N_{LASER^f}$ | $1.7 \times 10^{17} \frac{\text{photons}}{\text{sec}}$ | This value corresponds to 0.1 watts of average power at 3371$A^o$ in the ultraviolet. This is provided by the commercially available Avco Model C950 pulsed $N_2$ laser for example. |
| $N_{SCAT}$ | $2.9 \times 10^{19} (PPM \times 10^{-6})$ | Operation is at approximately Standard atmospheric density. |
| $\sigma_{RAMAN\ (SO_2)}$ | $4.8 \times 10^{-29} cm^2/ster$ | Using the data of Table I and a value of $2 \times 10^{-29} cm^2/ster$ for $\sigma_{RAMAN\ (N_2)}$. |
| $\sigma_{RAMAN\ (NO)}$ | $1.0 \times 10^{-29} cm^2/ster$ | |
| $\Delta R$ | 10 feet | Typical power plant plume diameter. |
| $A_T$ | $\frac{\pi}{4}(10)^2$ inches | Typical field optical systems are of this size. |
| $\epsilon_{pe}$ | 0.30 | RCA 8850 photomultiplier photocathode sensitivity in the ultraviolet. |
| $\epsilon_{op}$ | 0.10 | Typical transmission of a good monochrometer plus transfer optics. |
| $T_{\lambda_1} T_{\lambda_2}$ | 1.0 | This factor can vary from unity to zero depending on conditions. |

The experimental field apparatus described in Section V was designed to match as closely as possible the system parameters used in the above calculation. However, the laser output power was a factor of 4 less due to spatial and spectral filtering and there was a factor of 6 optical mismatch in the monochrometer system. This mismatch occurs because the combination of the 4 milliradian (2 mrad 1/2 angle) laser beam and the 60-inch focal length telescope produces a 6 mm image on the 1 mm wide monochromator entrance slit field stop. This loss of a factor of 6 can be corrected by the use of beam expansion and focusing optics in the laser transmitter.

The observed experimental Raman signals were a factor of 100 less than the calculation and a factor of 4 less than the actual field apparatus would be expected to produce. This factor of 4 discrepancy could be explained by a combination of uncertainties in cross-section absolute magnitude, optical transmission losses and the efficiency of the photoelectron counting process.

In addition to the absolute Raman signal strengths, the interference and possible overlap among the Raman scattering from the various molecular constituents of a combustion plume can also be calculated. Figure IV-2 shows the Raman spectrum expected from typical combustion gases at $300^{\circ}K$, including the $\Delta J = \pm 2$ rotational sidebands. The $\Delta J = 0$ components have been normalized to a signal of unit strength for $N_2$ in accordance with their concentration and scattering cross-section.

The $\Delta J = \pm 2$ components for $N_2$ are shown in Fig. IV-2, as previously indicated in Fig. II-2 and described in Section II. The amplitude of the $\Delta J = \pm 2$ components for the Raman lines of the other species are also shown approximately two orders of magnitude weaker than the strong $\Delta J = 0$ component. The width of the various $\Delta J = \pm 2$ components is, however, scaled proportional to the 1/2 power of the rotational constant ($B_e$ in Herzberg's notation)[3] for each specie.

The justification for this scaling can be seen by differentiating the expression for $N_J$ the number of molecules per rotational level.

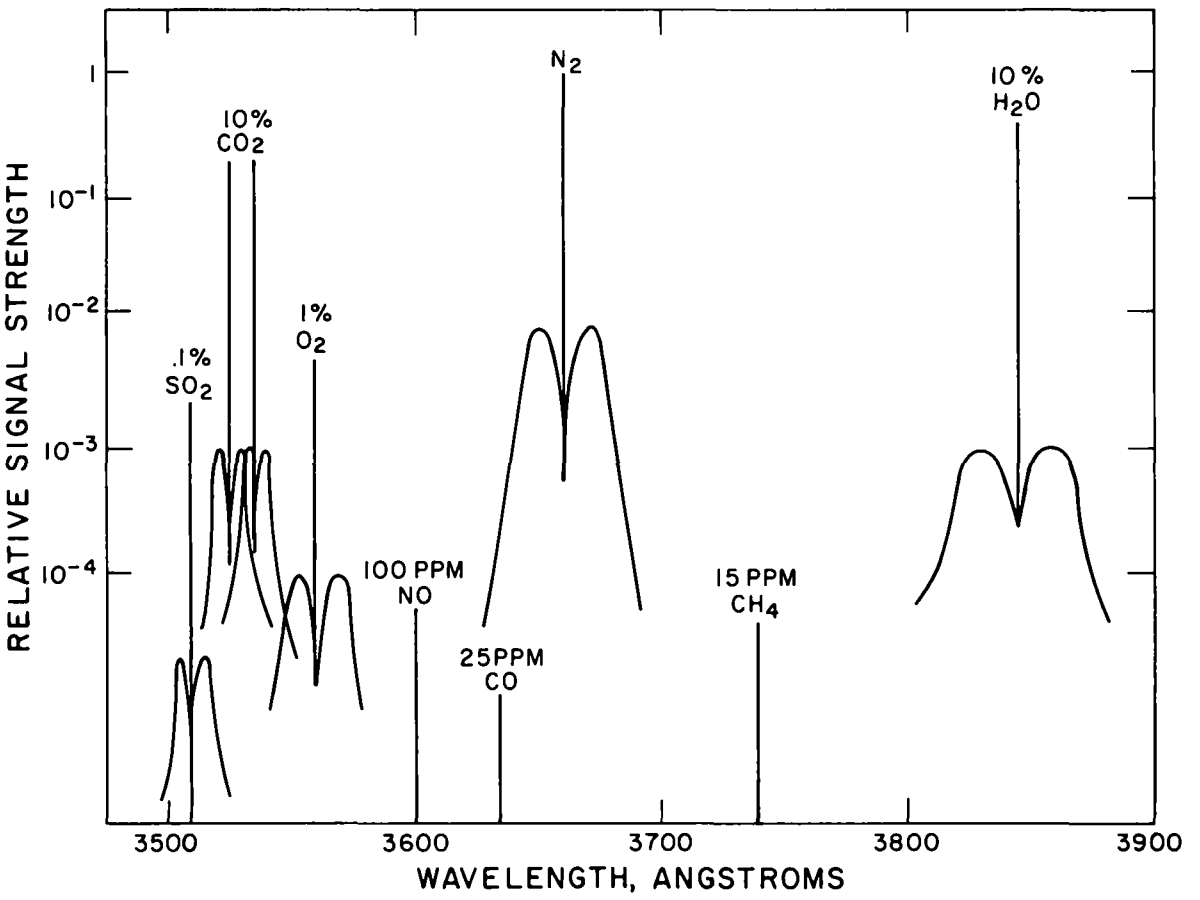


Fig. IV-2 Typical Raman spectrum from combustion gases using a 3371 Å laser source.

$$N_J = \frac{1}{Q}(2J+1)\, e^{-\frac{BJ(J+1)\,1.44}{T}}$$

$$\frac{dN_J}{DJ} = \frac{1}{Q}\left[2\, e^{-\frac{BJ(J+1)\,1.44}{T}} - \frac{1.44B}{T}(2J+1)^2\, e^{-\frac{BJ(J+1)1.44}{T}}\right]$$

and setting the derivative equal to zero and solving for $J_{Max}$ as a function of B

$$J_{Max} = \frac{1}{2}\left(\sqrt{\frac{1.4T}{B}} - 1\right)$$

$$\lambda_o - \lambda_{J_{Max}} = \Delta E \lambda_o^2 = B(4J+6)\lambda_o^2$$

$$\lambda_o - \lambda_{J_{Max}} \sim \sqrt{BT}$$

The widths of the $\Delta J = \pm 2$ sidebands were scaled according to $B_e = 2.01,\ 1.44,\ .39,\ 9.5\ cm^{-1}$ for $N_2$, $O_2$, $CO_2$ and $H_2O$, respectively.[3] ($SO_2$ was arbitrarily set equal to $CO_2$).

In summary the amplitudes of the sidebands in Fig. IV-2 are order of magnitude estimates whereas the widths are probably good to within a factor of 2. A more accurate and complete recalculation of Fig. IV-2, particularly as a function of temperature and relative concentration, would assist in defining the limits of the Raman method. However, NO is seen to be clearly free of interference and $SO_2$ lies more than 2 orders of magnitude above the sideband of $CO_2$. The CO Raman scattering on the other hand is less than the $N_2$ sideband for CO concentrations below about 250 PPM.

# V. EXPERIMENTAL FIELD APPARATUS

This section describes the remote pulsed laser Raman spectrometer which has been deployed and operated at the site of the Boston Edision Mystic Station Electric Power Plant.

## A. Laser

The laser used is a 3371 Å ultraviolet pulsed nitrogen laser, MOPA (Master Oscillator Power Amplifier). A small pulsed nitrogen laser is used as an oscillator to provide approximately 10 kW of peak power. The beam from the oscillator is passed through a mode control spatial filter which produces a beam with a divergence of 2 milliradians. The divergence controlled beam is then amplified in a second larger laser unit which is synchronized with the oscillator to within 1 nanosecond.

The output beam from the MOPA is passed through an interference filter designed to pass the 3371 Å laser line and block by at least 3 orders of magnitude the spontaneous emission lines in the nitrogen discharge which occur in the wavelength region of the Raman lines of interest. Steering mirrors are used to position the beam within the field of view of the telescope at the range of interest.

The resulting laser MOPA unit produces an output beam with the following characteristics:

| | |
|---|---|
| Peak Power | - 50 kilowatts |
| Pulse Repetition Rate | - 100 pulses per second |
| Pulse Duration | - 10 nanoseconds |
| Wavelength | - 3371 Å |
| Beam Divergence | - 2 milliradians |

## B. Receiver Optics

The optical system of the receiver is shown schematically in Fig. V-1. A 10-inch diameter, 60-inch focal length Newtonian telescope is used to collect the Raman backscattered photons produced by the outgoing laser pulse. Gross alignment is provided by the laser beam steering mirror.

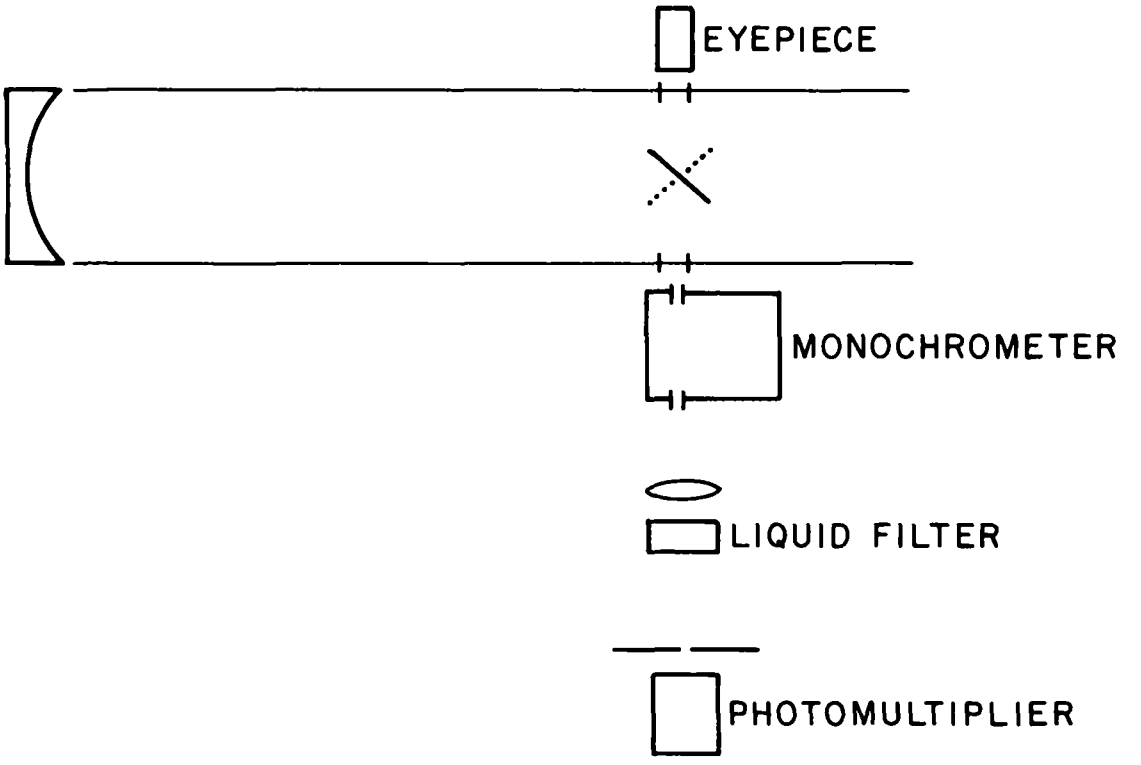


Fig. V-1 Optical system used in the power plant field experiment.

In practice, the telescope is first aligned so that the smoke plume is in view in the telescope eyepiece. The steering mirror is then adjusted for maximum returned signal on a strong Raman line such as $N_2$ at 3658 Å.

The photons collected by the telescope are passed through a Jarrell-Ash 1/4 meter monochrometer. This monochrometer has a measured resolution of 17 Å per mm, a transmission of 20% in the ultraviolet and a stray light rejection ratio reputed to be $10^{-3}$.

A lens focuses the exit slit of the monochrometer onto a field stop placed in front of an RCA 8850 photomultiplier. A liquid filter is placed adjacent to the lens. The liquid filter, a water solution of 2, 7 - dimethyl - 3, 6 - diazacyclohepta - 1, 6 - diene perchlorate in a quartz walled cell, has the property of essentially complete isotropic volume bulk absorption of 3371 Å but with nearly complete transparency at wavelengths of 3500 Å and longer. Figure V-2 is a plot of the filter's transmission vs wavelength. This filter is essential for blocking the strong on-frequency return at 3371 Å which is reflected from the smoke plume and which the Jarrell-Ash 1/4 meter monochrometer alone is not able to adequately reject. It is far superior in this regard than the best interference filters commercially available, both in transmission characteristics and in angle requirements.

C. Basic Receiver Electronics

The block diagram of Fig. V-3 shows the receiver detection electronics. The output from the RCA 8850 photomultiplier is sent directly to a 200 megacycle Hewlett-Packard 5248 counter. The counter discriminator threshold is set so that all photoelectron pulses produced by the photomultiplier are counted directly by the counter.

A synchronization pulse produced by the laser trigger circuit is suitably delayed (100 nanoseconds = 50 feet of range) and then sent to a gate generator which produces typically a 100 nanosecond gate pulse. This gate pulse is introduced into the counter in a manner such that the counter will count photoelectron pulses only during the time the gate is on. At all other times, between the laser pulses, the counter is inactivated and does not count the background and dark current photoelectron pulses produced.

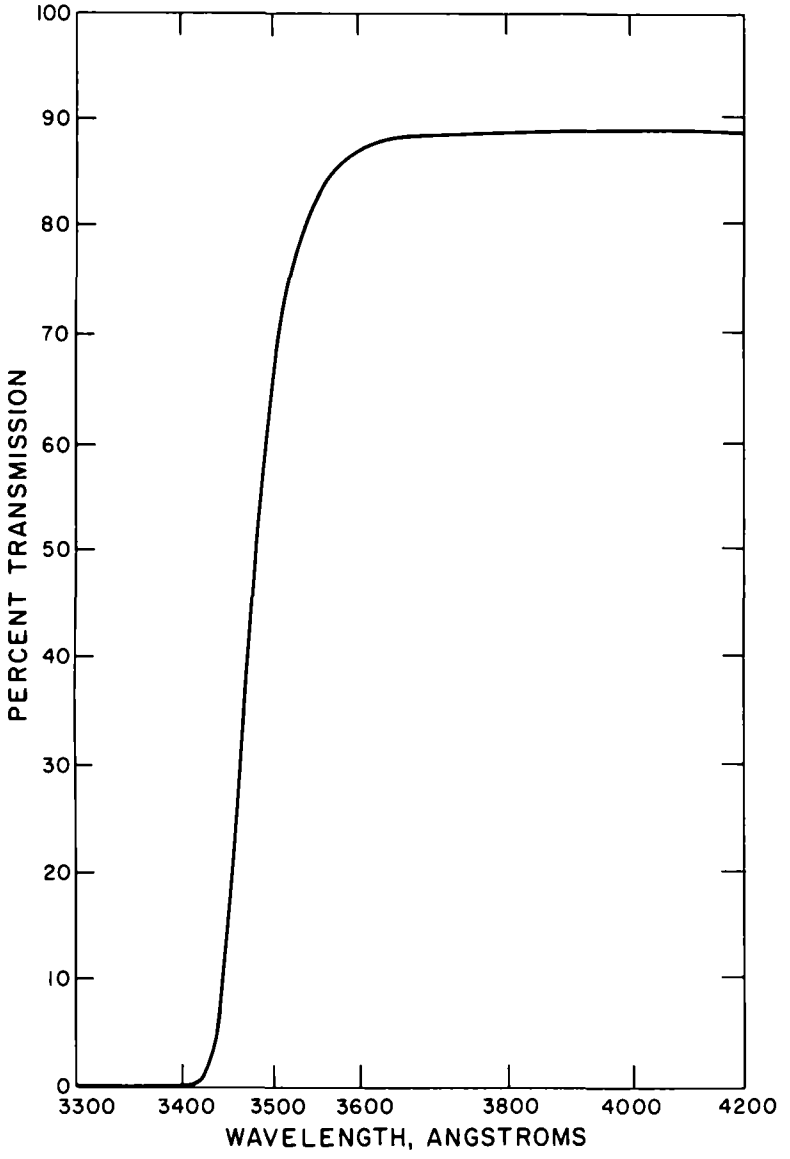


Fig. V-2 Transmission characteristic of the liquid filter used in the optical system of the field experiment.

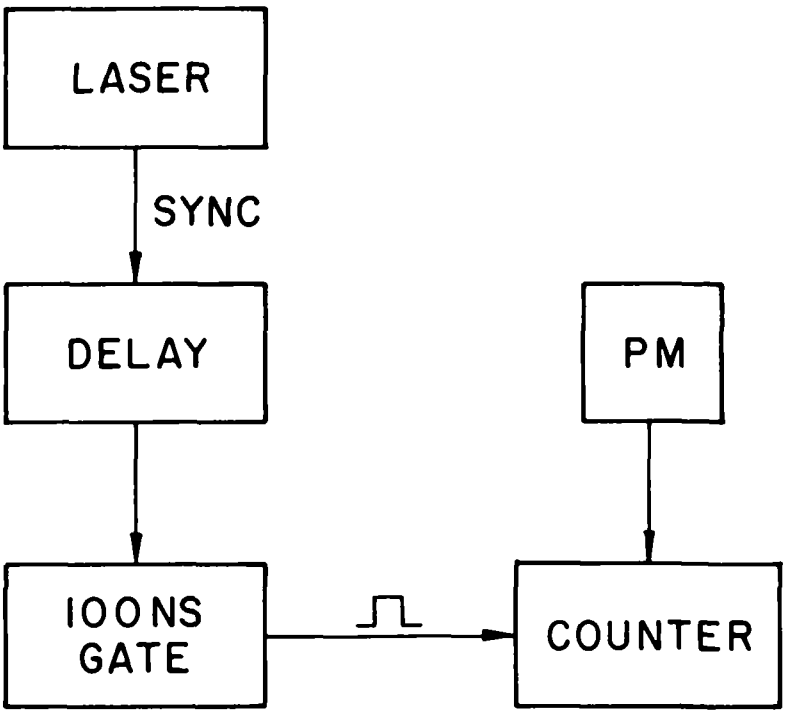


Fig. V-3 Schematic of the photon counting electronic detection system.

For the photomultiplier tube used, a typical dark current counting rate when ungated is 200 counts per second. When operating at 100 laser pulses per second, and with 100 nanosecond gate lengths the counting rate from dark current is reduced from 200 to $200 \times \frac{10^{-7}}{10^{-2}} = 2 \times 10^{-3}$ counts per second.

D. 10-Channel Receiver

To achieve the simultaneous measurement of an entire plume profile, as distinguished from the single point by point capability of the basic electronic system described above, a 10-channel (i. e., range gates) photon counting receiver was assembled and field tested satisfactorily.

As Fig. V-4 shows, the synchronization pulse from the laser trigger circuit is suitably delayed and then sent to a set of 10 gate generators which produce gate pulses, 30 nanoseconds wide and spaced 50 nanoseconds apart over a 500 nanosecond interval. These gates are introduced into AND circuits together with the photoelectron pulses from the photomultiplier. When a coincidence of a gate pulse and a photoelectron pulse occurs, a fixed increment of charge is added to the appropriate integrator. The D. C. voltage appearing at the output of each integrator is proportional to the number of photoelectrons received from each range cell. This device has enabled plume profiles to be obtained with one-tenth the integration time previously required.

E. Power Plant Site

The remote laser Raman spectrometer apparatus was placed in a van at the site of the Boston Edison Mystic Power Plant. The spectrometer van is approximately 500 feet from the base of the nearest stack, the top of which is 317 feet above sea level. The slant range from the laser to the stack plume was measured by the time of flight of the strong on-frequency return to be 1250 nanoseconds or 625 feet.

The position of the laser Raman spectrometer van relative to the power plant stacks is indicated in Fig. V-5 which is a sketch of the Mystic Station site plan.

Figure V-6 is a photograph showing the view of the power plant stacks from behind the spectrometer van.

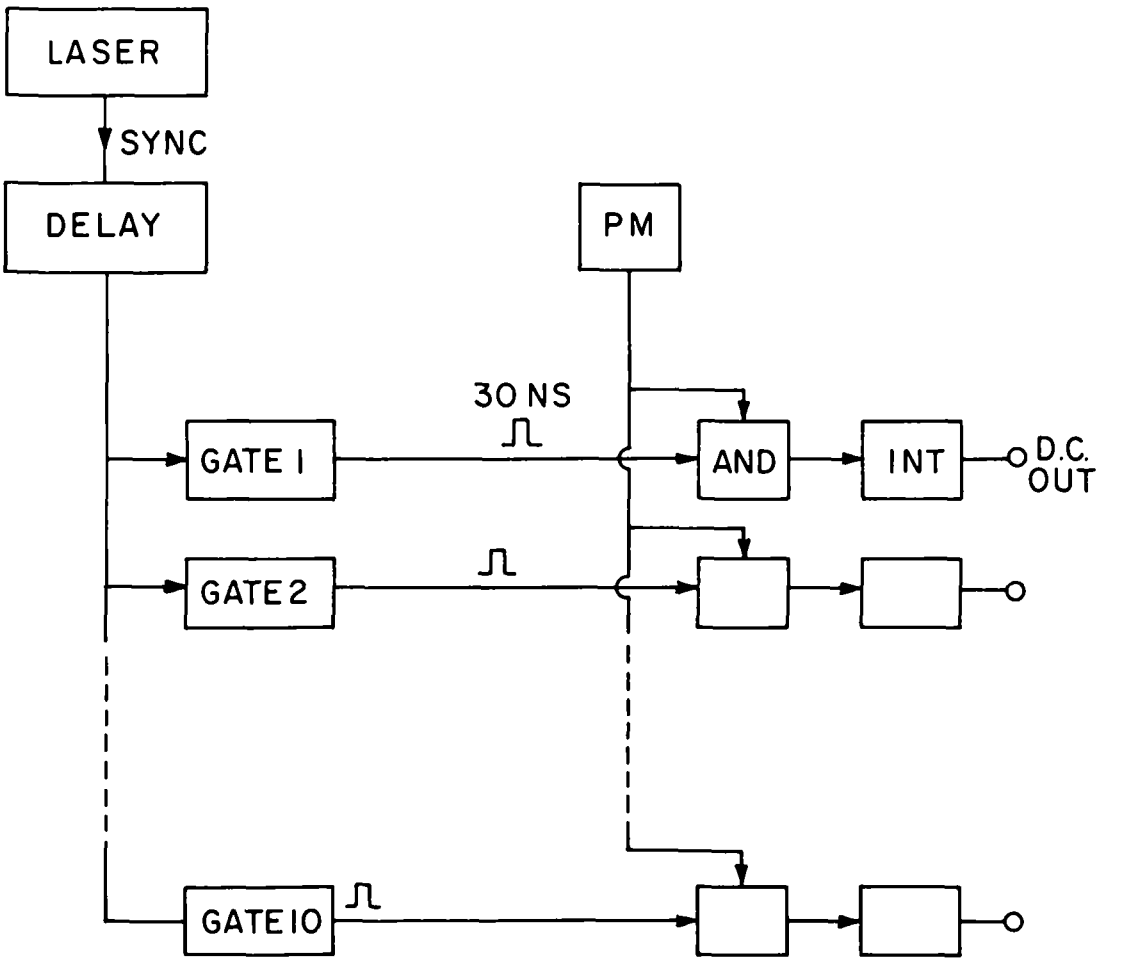


Fig. V-4 Schematic of the 10-channel photon counting detection system.

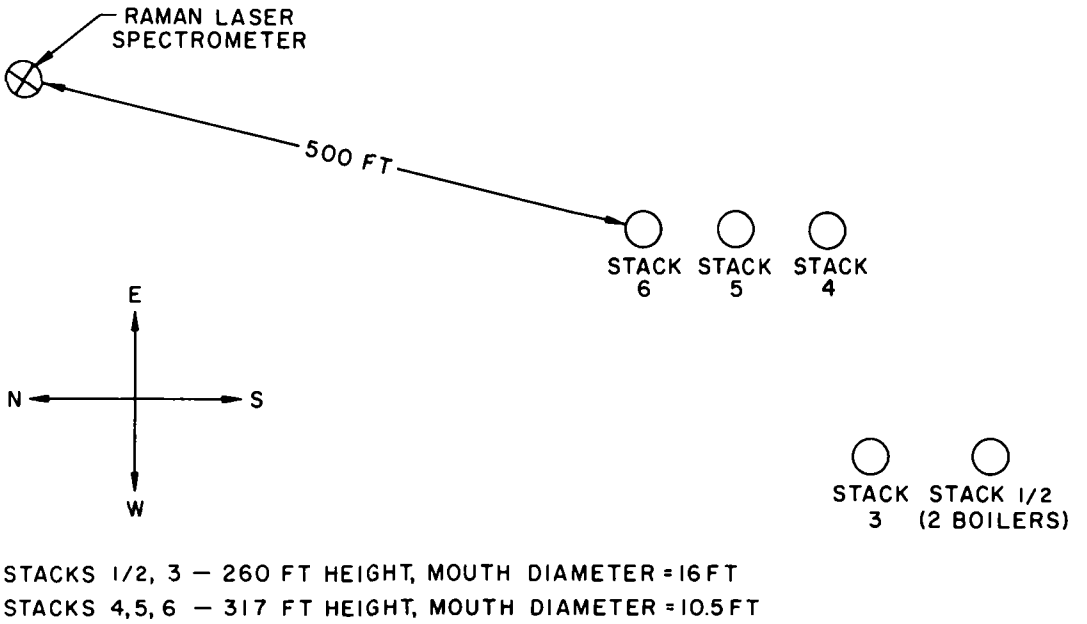


Fig. V-5 Plan view of the Boston Edison Mystic Station showing the position of the laser Raman spectrometer van.

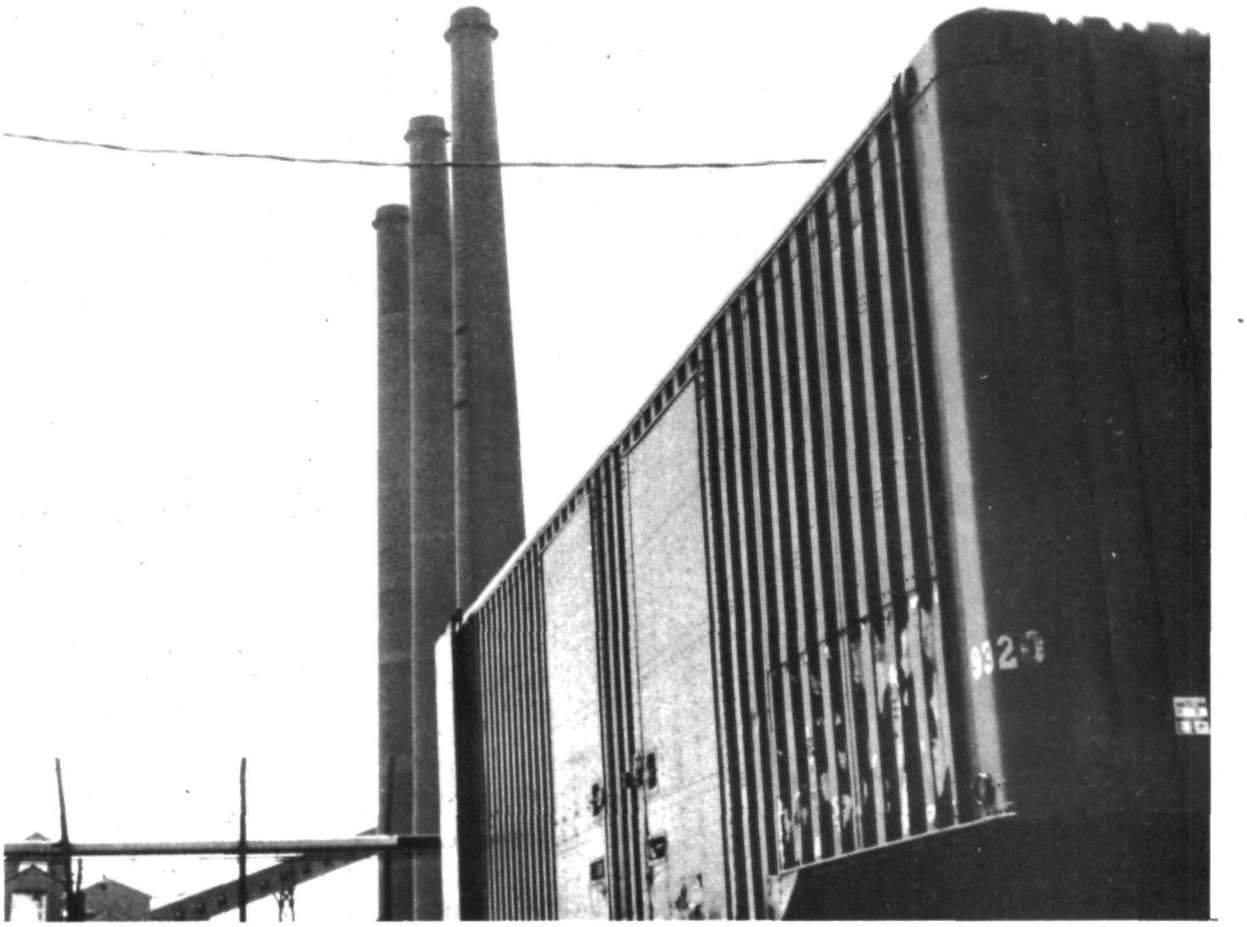

Fig. V-6 Photograph of spectrometer van at power plant site.

# VI. EXPERIMENTAL FIELD RESULTS

The apparatus described in Section V has been operated at the Boston Edison site and the results to date confirm our expectations of its capability, the current limitation being the selectivity of the 1/4-meter Jarrell-Ash monochrometer at about the 1% level of stray light rejection.

Useful data, however, were obtained with the existing experimental arrangement. Figures VI-1, VI-2 and VI-3 are typical spectral scans of the backscattered photons produced by the laser pulse which have been obtained at the power plant site. Figure VI-1 is a scan at a range of 425 feet, which is between the spectrometer van and the stack plume, and is a normal Raman air spectrum on a clear evening showing the $O_2$, $N_2$ and $H_2O$ Raman lines in approximately the expected ratios. This scan was obtained without an interference filter on the laser output.

Figure VI-2 is a spectral scan at a range of 625 feet, a range coincident with the stack plume position. In this spectral scan, four new lines have appeared at 3537 Å, 3577 Å, 3755 Å, and 3805 Å, in addition to the $O_2$, $N_2$ and $H_2O$ Raman lines at 3558 Å, 3658 Å and 3844 Å, respectively. These new lines were identified as emission lines in the laser discharge originating from the (1, 2), (0, 1), (1, 3) and (0, 2) transitions of the nitrogen second positive ($C^3\pi$ - $B^3\pi$) band system. The 3371 Å laser line originates from the (0, 0) transition of the same band system. The appearance of these relatively weak emission lines in the Raman spectrum when the range corresponds to the plume position indicates the enormously larger optical reflectivity of the plume as compared to "clear" ambient air.

The spectral scan of Fig. VI-3 resulted from the insertion of an interference filter in the outgoing laser beam which was designed to pass the laser line at 3371 Å and attenuate by at least 3 orders of magnitude wavelengths between 3500 Å and 3900 Å. Although the data of Fig. VI-3

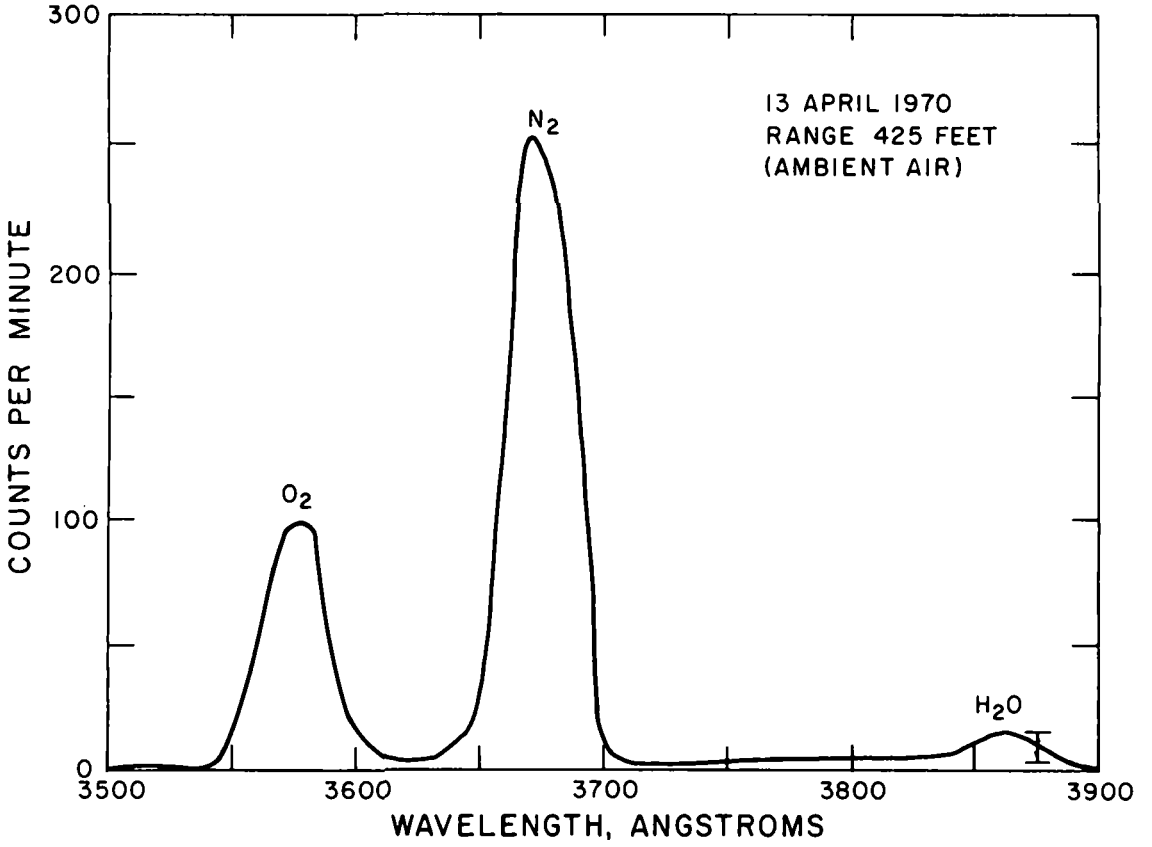


Fig. VI-1 Remote ambient air Raman spectrum

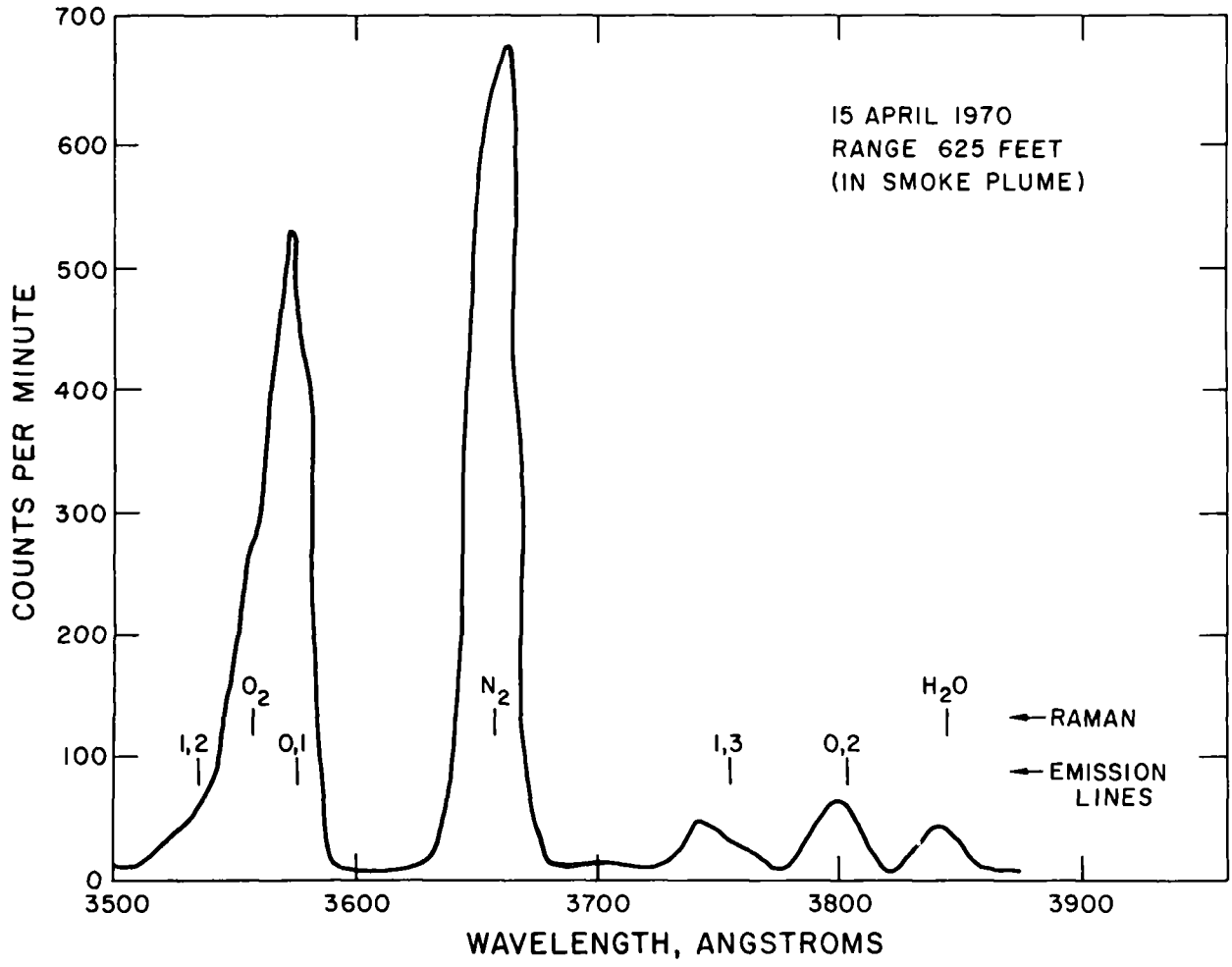


Fig. VI-2 Raman spectrum of smoke plume showing spontaneous emission lines.

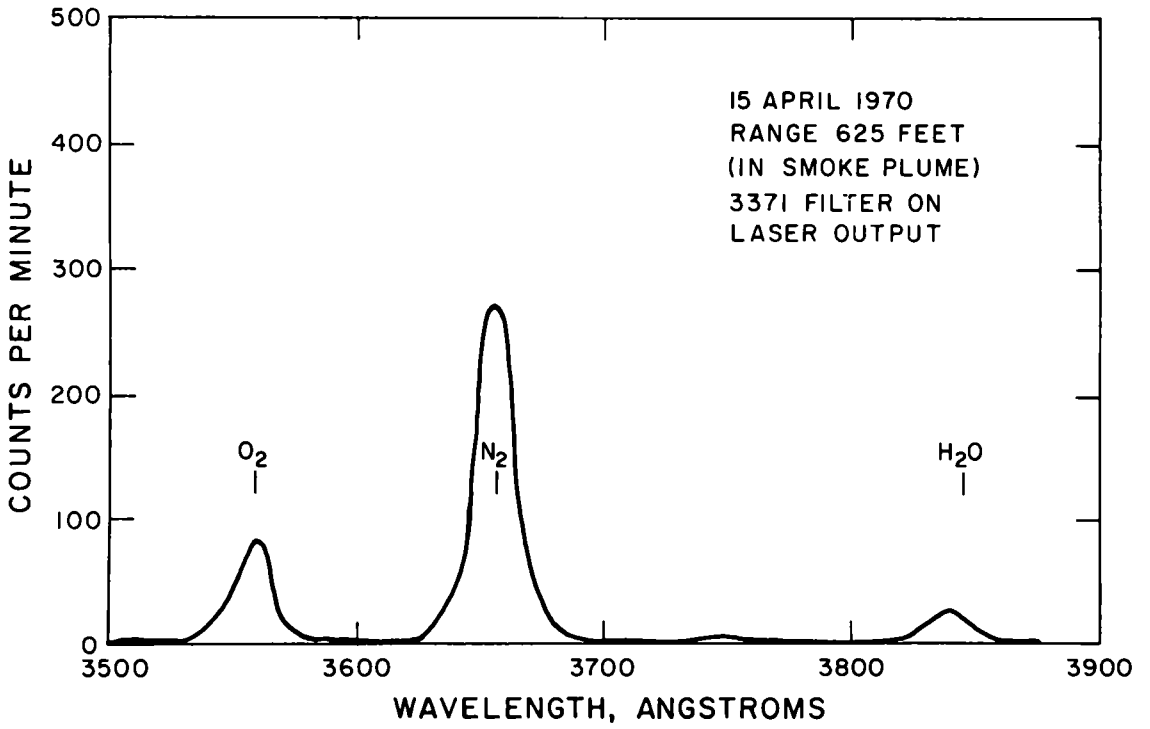


Fig. VI-3 Raman spectrum of smoke plume with spontaneous emission lines suppressed.

were obtained at the same 625 feet range position as Fig. VI-2, the addition of the filter eliminated the four new lines leaving just the $O_2$, $N_2$ and $H_2O$ Raman lines.

Scans as a function of range were obtained on the $O_2$, $N_2$ and $H_2O$ Raman lines. Data from a typical such scan are shown in Fig. VI-4 in which the Raman backscattered return multiplied by the square of the range is normalized to unity at a delay of 1400 nanoseconds and is plotted as a function of delay. The plume position is at approximately 1600 nanoseconds. Data with less delay represent scattering from in front of the plume, data with more delay represent scattering from behind the plume.

The following conclusions and observations can be drawn from Fig. VI-4:

(1) The ratio of the $N_2$ (or $O_2$) Raman signal level behind the plume to the $N_2$ (or $O_2$) Raman signal level in front of the plume gives a direct measure of the two-way plume transmission. A solid line is drawn through the points for the $N_2$ Raman signals showing a drop to 0.2 which is a direct measure of the two-way plume transmission. The one-way transmission is $(0.2)^{1/2}$ or 45%.

(2) The $O_2$ signal level at the delay time corresponding to the plume position is less than the $N_2$ signal level at the same delay time.

(3) The $H_2O$ signal level at the delay time corresponding to the plume position is greater than the $N_2$ signal level at the same delay time.

Observations (2) and (3) above show the expected decrease in $O_2$ content of the plume and an increase in water vapor due to combustion of the hydrocarbon fuel. The uncertainty in the data for water vapor, while large, is still adequate to support the above conclusions. The water vapor to $N_2$ (and $O_2$) ratio before and after the plume is the same within the precision of the measurement.

Similar data have been obtained with the 10-channel receiver, representing the simultaneous measurement of an entire plume profile. In addition, with the same receiver, scattering from the plume position was obtained at 3524 Å, the Raman wavelength corresponding to $CO_2$. This $CO_2$ data is also shown in Fig. IV-4 normalized by setting the value at 1600 ns equal to 1.0 and the average of all the other range cells equal to zero. The conclusion is that a significant $CO_2$ signal appears only at the plume position.

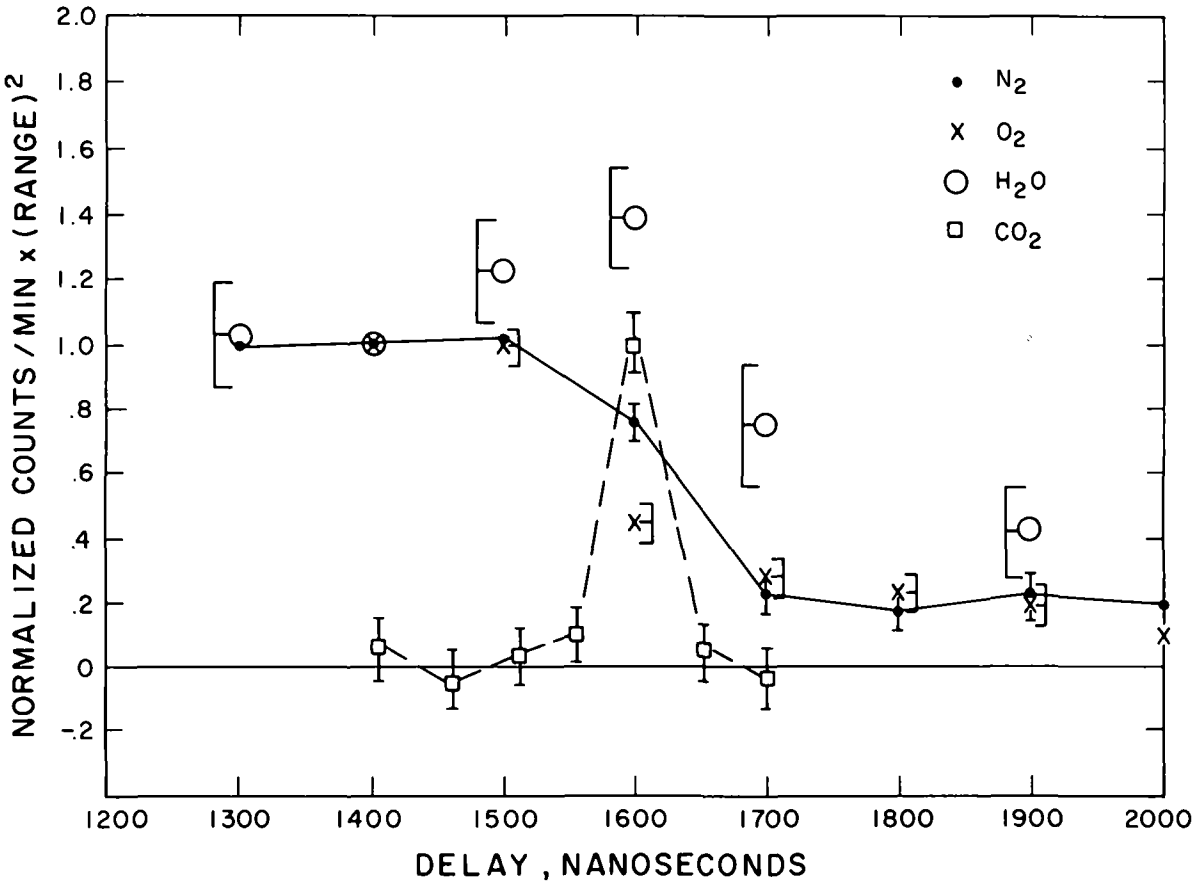


Fig. VI-4 Plume profile showing normalized Raman scattering from $N_2$ $O_2$, $CO_2$ and $H_2O$.

A. Flue Gas Analytical Measurements

The Walden Research Company was engaged to make analytical measurements by conventional methods on the power plant exhaust gases. One such set of tests were conducted by Walden on the evening of 2 July 1970. The exhaust gases were sampled in the duct between the electrostatic precipitator and the direct draft fan. The Orsat analysis showed $CO_2$ at 9.1% and $O_2$ at 9.7% indicating the presence of about 50% excess air. The $NO_X$ Phenal Disulfonic Acid analysis ranged from 155 to 234 PPM. The $SO_2$ measurement failed to work because of a leak in the sampling system used. It was intended that such analytical measurements be made coincident with the laser Raman measurements to validate the technique.

B. Remote Laser Hygrometry

Measurement of water vapor profiles in ambient air was accomplished incidental to the plume study. Figure VI-5 shows the ratio of the Raman signal from $H_2O$ to the Raman signal from $O_2$ plotted as a function of range. Each point in this case was obtained separately and the entire set of data was obtained over a half hour period. The error bars represent the photostatistics associated with the collection of about 100 photoelectrons for each point. The average of the data is compared with that calculated from Weather Bureau temperature and relative humidity data supplied from Logan Airport and the cross-sections for $H_2O$ and $O_2$ as given in Table I. The ratio of the calculated value to the experimental average is .82. Similar comparisons on three other nights gave comparison ratios of 1.06, 1.06 and 1.40. Exact agreement is not expected since the laser and Weather Bureau measurements were not precisely coincident in either time or space. However, the close correlation indicates that remote laser hygrometry is feasible and might be used to improve meteorological data acquisition.

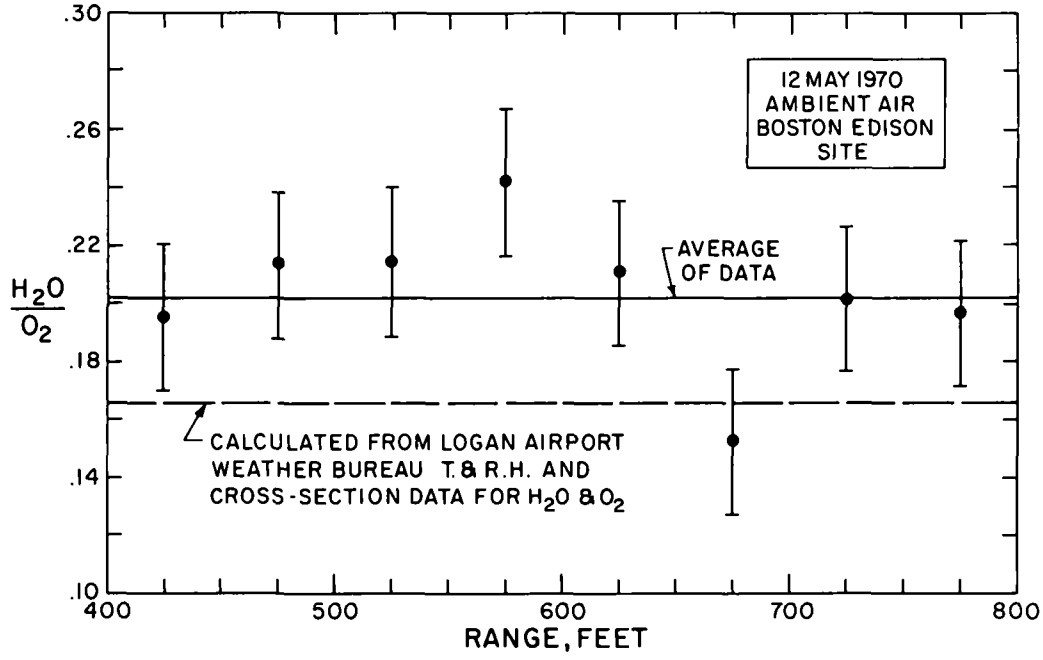


Fig. VI-5 Water vapor to oxygen Raman ratio in ambient air.

## VII. CONCLUSIONS

Calculability of Raman Returns - The cross-sections for NO and $SO_2$ Raman scattering have been measured and are now known. The Raman returns from plumes containing these molecules can now be calculated with precision. The detection of Raman scattering from 100 PPM NO and $SO_2$ is theoretically practical with reasonable system components.

Molecular Interference - For concentrations of NO and $SO_2$ of 100 PPM and above, it has been established theoretically that the Raman scattering from the other molecular species in the plume ($CO_2$, $O_2$, $N_2$, $H_2O$ and CO) will not interfere with the measurement if an appropriate high performance monochrometer is used.

Raman Scattering Obtained Remotely from Plume - Raman spectra of $N_2$, $O_2$, $H_2O$ and $CO_2$ have been obtained experimentally from a power plant plume at a range of 625 feet.

Quantitative Profiles of Plume Species - Quantitative density profiles of molecular species in the plume can now be routinely obtained. For example, the fact the plant was operating with 50% excess air was detected by the ratio of the $O_2$ Raman to the $N_2$ Raman observed in the plume and later confirmed by an Orsat analysis of the stack gases.

Plume Transmission Measured - The two-way plume transmission was easily measured by directly comparing the ratio of the $N_2$ (or $O_2$) Raman signal level behind the plume to the $N_2$ (or $O_2$) Raman signal level in front of the plume.

Establishment of Preferred Definition of Emission Standard - The simultaneous measurement of $CO_2$, $SO_2$ and NO can be used to unambiguously obtain the ratio of $SO_2$ to $CO_2$ and NO to $CO_2$ independent of the optical transmission characteristics of the plume or the amount of excess diluent air passed up the stack. Specifying the $SO_2/CO_2$ and $NO/CO_2$ ratio might prove to be a practical, easily measureable, and legally enforceable standard.

Simultaneous Range Information Required - Approximately 10 simultaneous range data points are required to establish unambiguously the position of plume, the transmission through the plume, and the relative concentration of molecular constituents within the plume.

No Interference Experimentally Observed - No interference with the molecular Raman scattering has been experimentally observed down to an equivalent pollutant level of 10,000 PPM.

Fluorescence and Particulate Raman Interference - The possible interference from flourescence and Raman scattering from the solid and liquid material in the plume, such as ash, dust, and aerosols, cannot as yet be estimated with sufficient precision. The existance of interference from such sources can only be determined experimentally on an actual source of emissions such as a power plant. Reasonably sophisticated equipment must be used.

100 PPM Feasibility Not Resolved - Raman returns from NO and $SO_2$ have not yet been observed experimentally from the power plant plume. The detection by Raman scattering of NO and $SO_2$ in the 100 to 1000 PPM concentration range has therefore not yet been proven feasible. There still exists the possibility that fluorescence and Raman scattering from foreign materials may limit the effectiveness of the technique.

Feasibility of Raman Scattering for Remote Hygrometry is Indicated: The measurement of remote water vapor profiles in ambient air was accomplished incidental to the plume study. The data obtained were consistent with Weather Bureau records of the humidity in the Boston area at the time of the tests. This technique may be of use for meteorological support of air pollution control.

# VIII. RECOMMENDATIONS

Additional Field Experiments with Improved Monochrometer - More experimental field work with an improved instrument is required to resolve the question of the feasibility of the Raman method for measurement of NO and $SO_2$ in the 100 PPM concentration range. The work to date utilized a standard 1/4-meter Jarrell-Ash monochrometer with a stray light rejection ratio of 1 part in several hundred. A Spex Model 1702 monochrometer with a stray light rejection ratio of 1 part in $10^4$ to $10^6$ has been purchased by Avco for its laser Raman program. An instrument of this caliber, used in conjunction with the laser and other equipment assembled at the power plant site, should enable a satisfactory resolution of the question of feasibility.

## REFERENCES


1. Smekel, A., Naturwiss 11, 873 (1923).

2. Sharma, Ramesh, Avco Everett Research Laboratory, private communication.

3. Herzberg, G., "Molecular Spectra and Molecular Structure, Infrared and Raman Spectra of Polyatomic Molecules," D. Van Nostrand Co. (1966).

4. Widhopf, G. F. and Lederman, S., "Specie Concentration Measurements Utilizing Raman Scattering of a Laser Beam," Polytechnic Institute of Brooklyn, Report No. 69-46.

5. Cooney, John, National Center for Atmospheric Research, private communication.

6. Derr, Vernon, ESSA, Boulder, private communication.

7. Leonard, D.A., Journal of Applied Physics, 41, 4238 (1970).

# APPENDIX

## MEASUREMENT OF NO AND $SO_2$ RAMAN SCATTERING CROSS-SECTIONS

The recent growing interest in air pollution control has motivated a search for more effective means of remote monitoring of atmospheric pollutants. One possibility is remote laser Raman scattering. The observation of Raman backscatter at ranges up to several kilometers in the atmosphere has previously been reported for nitrogen and oxygen[A-1, A-2] and water vapor.[A-3, A-4]

The purpose of this letter is to report laboratory measurements of Raman scattering cross-sections at 337.1 nm for gaseous nitric oxide (NO) and sulfur dioxide ($SO_2$). Measurements were made at both $90^o$ and $180^o$. Remote pollution monitors using laser Raman backscattering require knowledge of these cross-sections for instrument design and calibration.

A schematic of the apparatus used for the $90^o$ measurements is shown in Fig. A-1. The laser source consisted of a 100 kilowatt peak power, 10 nanosecond 337.1 nm pulsed nitrogen laser[A-5] operating at 100 pps. The output from the laser was filtered with the interference filter, $F_1$, which passed the laser line at 337.1 nm and attenuated the spontaneous emission occurring at the Raman wavelengths in the laser discharge by more than a factor of one thousand. After filtering, the laser beam was focussed at the center of a test cell containing the gases of interest.

After passing through a long pass filter, $F_2$, the focal region of the test cell was imaged onto the slit of a half-meter monochrometer. The filter, $F_2$, was designed to pass the Raman lines but attenuate the 337.1 nm laser line by a factor greater than one thousand.

After passing through the monochrometer the signal was detected by an RCA 7265 photomultiplier and displayed on a Textronic 585 oscilloscope, the latter being triggered by a sync pulse from the laser. The trace of the oscilloscope was viewed with a 1P28 photomultiplier, the

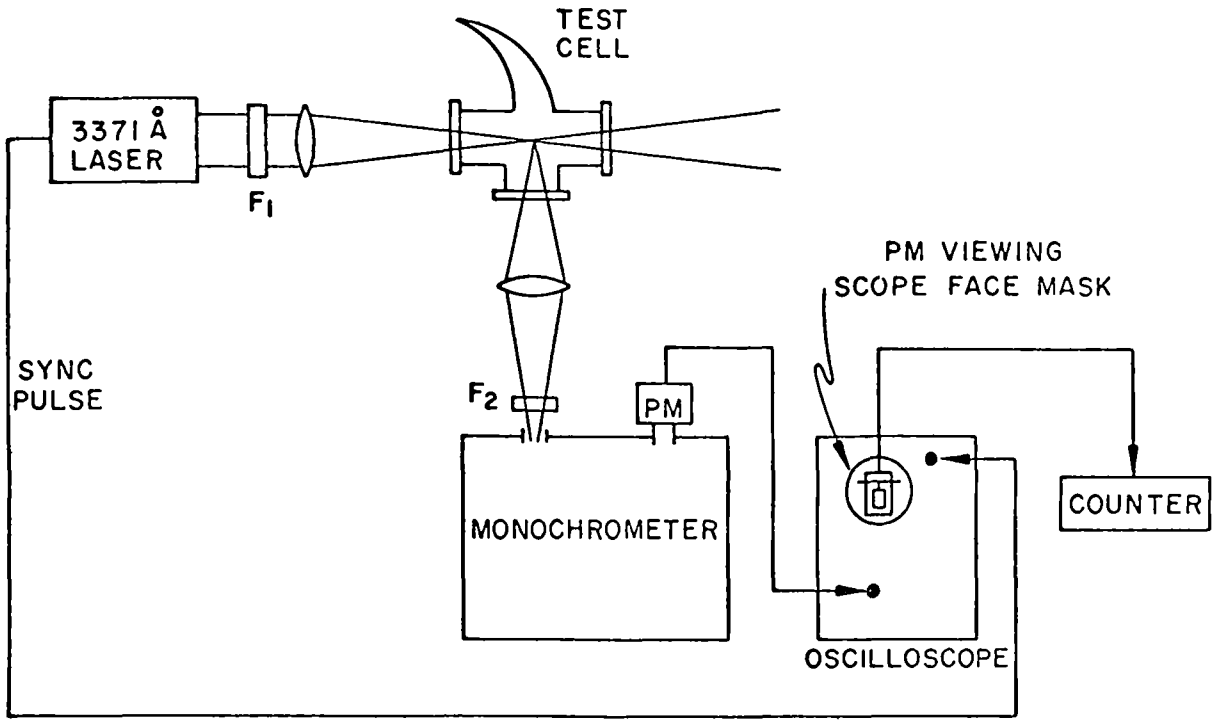


Fig. A-1 Schematic of Experimental Arrangement for 90° Cross-Section Measurements

output of which went directly to a counter. A mask on the face of the oscilloscope prevented the 1P28 photomultiplier from seeing the baseline of the trace.

However, an aperture in the mask placed below the trace permitted viewing the pulses originating from the monochrometer photomultiplier during a 100 nanosecond interval which includes the 10 nanosecond laser pulse. These pulses are recorded as individual counts on the counter. This method of coincidence counting is described in Ref. A-6.

The physical set-up for the $180^{o}$ measurements is shown in Fig. A-2. The additional field stop is arranged so that essentially all the light backscattered from the focal region within the test cell is transmitted; whereas laser light scattered from the objective lens and the test cell windows is strongly attenuated by the field stop.

The measurements were made with mixtures of NO with $N_2$ and $SO_2$ with $N_2$ in the test cell. The desirability of using $N_2$ Raman scattering as a normalizing standard[A-7] for atmospheric Raman spectroscopy required the measurement of the NO and $SO_2$ cross-sections relative to $N_2$. No attempt was made to measure absolute cross-sections. However, the results were consistent with the value of $2 \times 10^{-29}$ $cm^2$/ster for $N_2$.[A-8]

Typical data obtained with an equal molar mixture of NO and $N_2$ at one atmosphere total pressure are shown in Fig. A-3 as a plot of counts per minute as a function of wavelength. The counting rate was purposely maintained much smaller than the 6000 pulse-per-minute repetition rate of the laser to minimize the possibility of multiple photon events during one gate interval. The peaks at 359.9 and 365.8 nm correspond to the vibrational Raman Stokes shifts for NO and $N_2$, respectively. Similar data were obtained for mixtures of $SO_2$ with $N_2$.

The results for both $180^{o}$ and $90^{o}$ are best fit by a NO to $N_2$ Raman cross-section ratio of $0.5 \pm 0.1$ and a $SO_2$ to $N_2$ Raman cross-section ratio of $2.4 \pm 0.3$. Since this measurement includes essentially only $\Delta J = 0$ contributions, these cross-section ratios are for the $\Delta J = 0$ transitions only. A careful analysis of the wings of the Raman lines would be required to determine the relative strengths of the $\Delta J = \pm 2$ transitions.

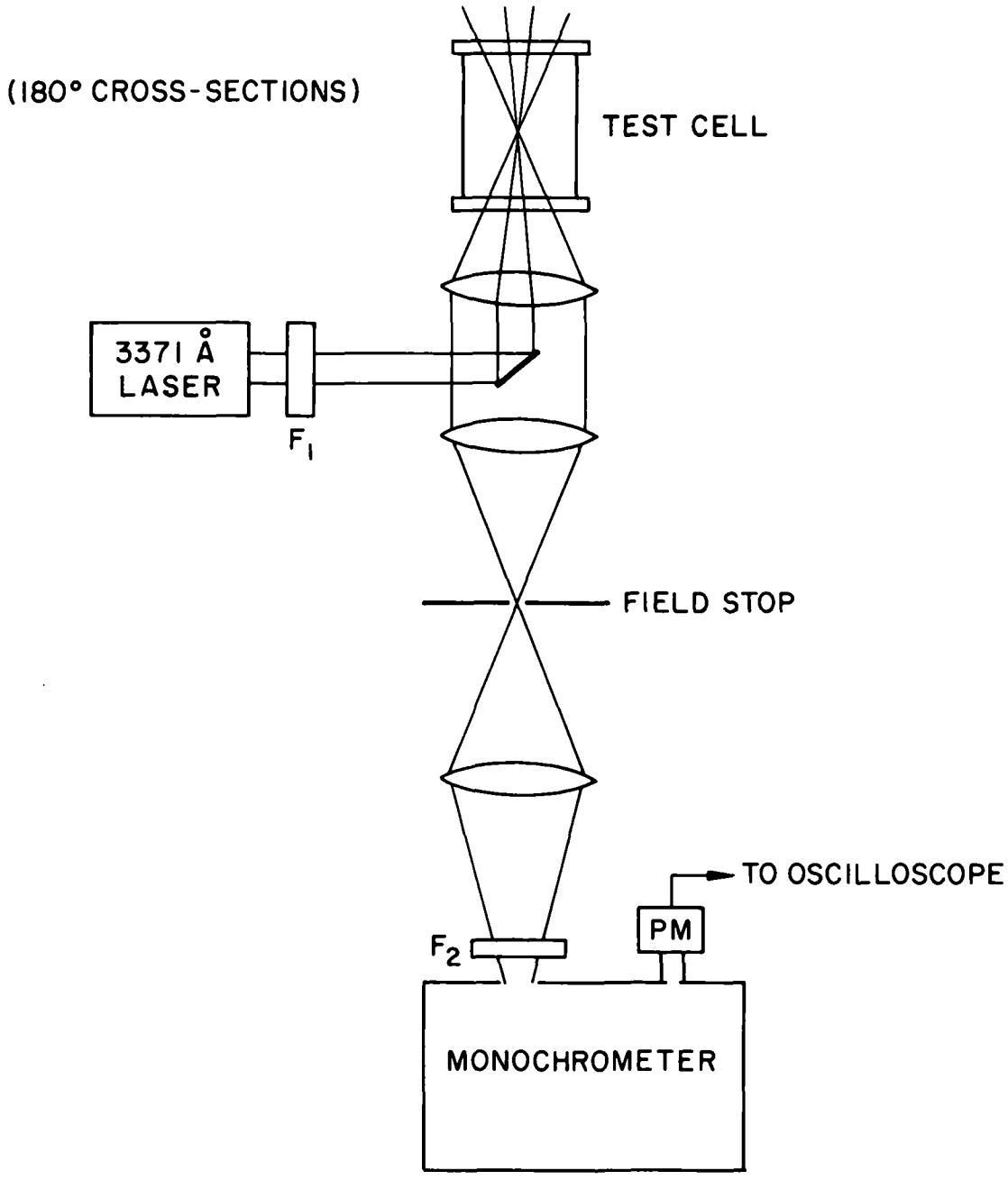


Fig. A-2 Schematic of Experimental Arrangement for 180° Cross-Section Measurements

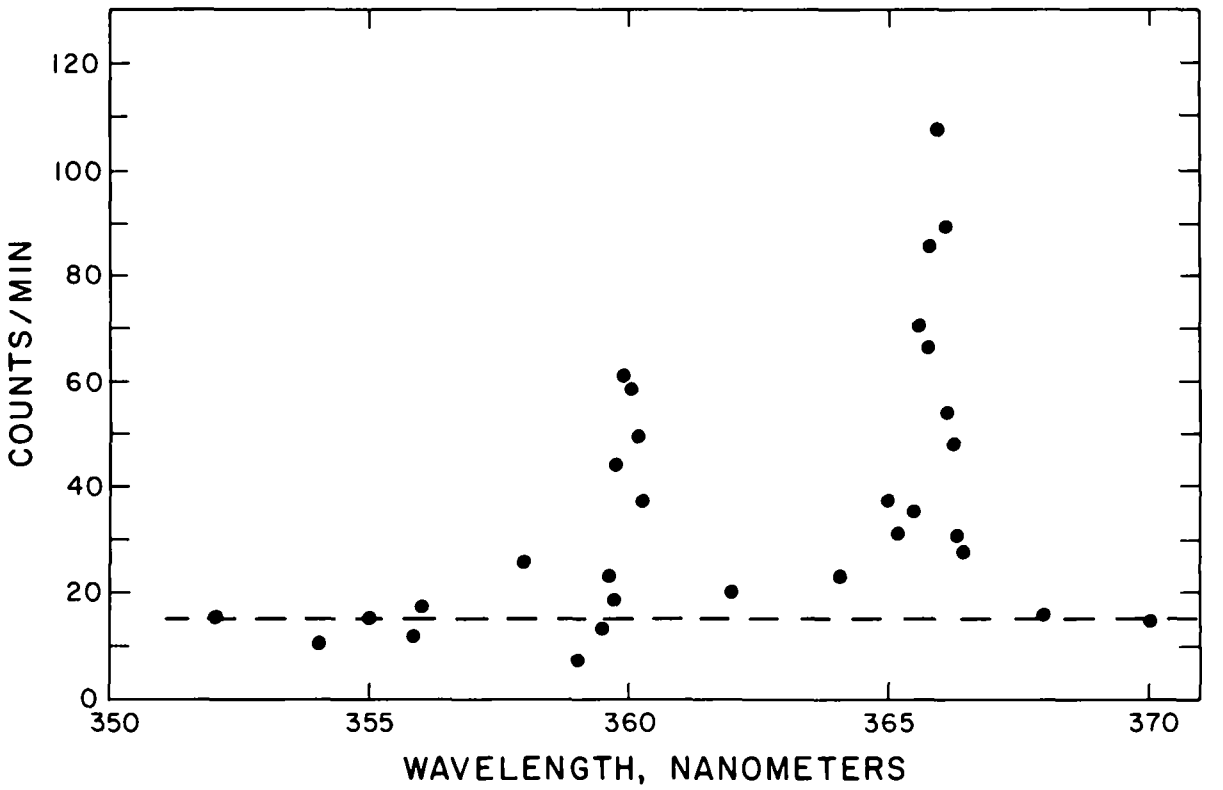


Fig. A-3 Spectral Scan of 50% NO - 50% $N_2$ Mixture showing the Relative Strength of the NO Line at 3599 Å and the $N_2$ Line at 3658 Å

## APPENDIX REFERENCES


A-1. Leonard, D. A., Nature 216, 142 (1967).

A-2. Cooney, J. A., Appl. Phys. Letters 12, 40 (1968).

A-3. Cooney, J. A., Nature 224, 1098 (1969).

A-4. Melfi, S. H., Lawrence, J. D. Jr., and McCormack, M. P., Appl. Phys. Letters 15, 295 (1969).

A-5. Leonard, D. A., Laser Focus 3, 26 (1967).

A-6. Lewis, I. A. D., and Wells, F. H., Millimicrosecond Pulse Techniques, 2nd Edition (McGraw-Hill, N. Y., 1955) p. 263.

A-7. Recommended by the Standards Committee of the Group on Laser Atmospheric Probing, National Center for Atmospheric Research, Boulder, Colorado.

A-8. Stansburg, E. J., Crawford, M. F., and Welsh, H. L., Can. J. Phys. 31, 954 (1953).